2012-05-28

Effect of the vanadium(V) concentration on the spectroscopic properties of nanosized europium-doped yttrium phosphates

DALTON TRANSACTIONS, CAMBRIDGE, v. 41, n. 20, pp. 6310-6318, MAY 28, 2012

Dalton Transactions

Cite this: *Dalton Trans.*, 2012, **41**, 6310

www.rsc.org/dalton

PAPER

Effect of the vanadium(v) concentration on the spectroscopic properties of nanosized europium-doped yttrium phosphates†

Jonathan Carvalhaes Batista, Paulo Cesar de Sousa Filho* and Osvaldo Antonio Serra

Received 17th February 2012, Accepted 26th March 2012
DOI: 10.1039/c2dt30380a

Nanosized rare earth phosphovanadate phosphors ($Y(P,V)O_4:Eu^{3+}$) have been prepared by applying the organic–inorganic polymeric precursors methodology. Luminescent powders with tetragonal structure and different vanadate concentrations (0%, 1%, 5%, 10%, 20%, 50%, and 100%, with regard to the phosphate content) were then obtained for evaluation of their structural and spectroscopic properties. The solids were characterized by scanning electron microscopy, X-ray diffractometry, vibrational spectroscopy (Raman and infrared), and electronic spectroscopy (emission, excitation, luminescence lifetimes, chromaticity, quantum efficiencies, and Judd–Ofelt intensity parameters). The solids exhibited very intense $^5D_0 \rightarrow {}^7F_J$ Eu^{3+} transitions, and it was possible to control the luminescent characteristics, such as excitation maximum, lifetime and emission colour, through the vanadium(v) concentration. The observed luminescent properties correlated to the characteristics of the chemical environments around the Eu^{3+} ions with respect to the composition of the phosphovanadates. The Eu^{3+} luminescence spectroscopy results indicated that the presence of larger vanadium(v) amounts in the phosphate host lattice led to more covalent and polarizable chemical environments. So, besides allowing for control of the luminescent properties of the solids, the variation in the vanadate concentration in the obtained $YPO_4:Eu^{3+}$ phosphors enabled the establishment of a strict correlation between the observable spectroscopic features and the chemical characteristics of the powders.

Introduction

For almost a half of a century, rare earth (RE)-based phosphors have by far been the most important luminescent materials with application in many technological fields.[1,2] Since lanthanoid ions present partially filled 4f orbitals protected from the chemical environment by the outer 5s and 5p electrons, their unique line-type f–f electronic transitions, mainly in their trivalent state, result in practically monochromatic emissions, which has enabled their use for light generation in several high-performance devices.[2] For example, RE-compounds are still the best phosphors for the generation of the three primary colours (red, green, and blue, RGB) in illumination (such as compact fluorescent lamps) and visualization (cathode ray tubes, field emission displays, and plasma display panels) technologies.[3,4]

Particularly, oxossalt phosphors such as phosphates, vanadates, borates, and niobates, among others, are quite important within the luminescent materials field. This is because they display very high physico-chemical stability, especially against high-temperatures or high-excitation energies, not to mention their very high luminescence efficiencies.[4] Such properties make these compounds applicable as vacuum ultraviolet phosphors (VUV, $\lambda_{exc} < 200$ nm), as they can exhibit very high excitabilities around 142 and 172 nm, which are the main lines provided by the xenon plasma employed in such devices. Therefore, these properties enable their application in Hg-free fluorescent lamps, by using rare gas mixtures instead of mercury, or in the development of large high-resolution plasma display panels.[5] On the other hand, the luminescence processes in such matrices can be considerably complex. This is because, although the optical transitions are only weakly affected by the occupied chemical environment, the non-radiative transitions are quite dependent on the characteristics of the matrix, such as composition, electronic structure, and particle size.[6] Moreover, in these cases vibrational energies of the matrix are relatively high (>800 cm^{-1}), which can lead to effective vibronic interactions with the metal states, thereby resulting in intense quenching processes. In this way, the viability of applying an oxossalt-based phosphor containing RE ions depends on the study of several spectroscopic, compositional and structural parameters, so that the advantages and disadvantages of their use as light emitters can be weighted.

In this sense, RE phosphate and vanadate phosphors have been widely applied and studied as commercial luminescent materials, as in the case of the utilization of the classic green and red phosphors $LaPO_4:Ce^{3+},Tb^{3+}$ and $YVO_4:Eu^{3+}$ in cathode ray tubes and fluorescent lamps. RE vanadates are quite relevant in the lighting field, since they have been used as phosphors in

Rare Earth Laboratory, Faculdade de Filosofia, Ciências e Letras de Ribeirão Preto, University of São Paulo, Av. Bandeirantes, 3900, 14040-901 Ribeirão Preto, SP, Brazil. E-mail: pcsfilho@usp.br; Fax: +55 16 3602 4838; Tel: +55 16 3602 4376

† Electronic supplementary information (ESI) available: Additional luminescence spectra, luminescence lifetime decay curves, and additional SEM micrographs. See DOI: 10.1039/c2dt30380a

high-pressure Hg lamps, mainly because of their luminescence efficiency even at high operating temperatures (300 °C).[3,4] Furthermore, vanadate phosphors have also been successfully employed in the manufacture of efficient high-power polarizing prisms[7] and active laser materials such as YVO_4:Nd^{3+},[3,4,8] as well as scintillators in medical image detectors.[9]

The RE vanadates are isostructural to the RE phosphates, so they have monoclinic (monazite) or tetragonal (xenotime/zircon) crystal structures,[10] which makes the development of mixed phosphovanadate phosphors with a number of advantageous luminescent properties possible. For instance, the partial replacement of PO_4^{3-} with the VO_4^{3-} species can afford improved stability and high-temperature luminescence characteristics,[11] besides allowing for the control of the emission colour, due to the higher intensity of the vanadate blue emissions when this group is diluted, and of the luminescence lifetime. Since the emission processes are not controlled by the nature of the host lattice and the activator only, the crystal morphology, size, and surface area, as well as crystallite defects, agglomeration, and homogeneity also play important roles in the decay mechanisms of the excited species.[1,4–6] Thus, in order to control the architecture and spectroscopic features of these compounds, countless methodologies have been developed for their synthesis, such as the incorporation of the phosphor into colloidal silica spheres or the obtainment of SiO_2@YVO_4 core–shell systems,[12] their preparation by high-temperature solid state reaction,[13] electron spinning methods,[14] sol–gel and polymeric precursors methodologies for the obtainment of both powder[15–17] and thin film[18] phosphors, lithography processed luminescent films,[19] as well as hydrothermal,[11,20] colloidal,[21] and template-directed[22,23] precipitations, among others.

Improving the quality of phosphovanadate compounds as luminescent materials remains an essential research topic, since the optimization of the matrix components (mainly lanthanum, yttrium, or gadolinium), the phosphorus/vanadium ratio, and the activator concentration is crucial for the applicability of these solids in various devices. In this context, this work aims at the synthesis and characterization of Eu^{3+}-doped yttrium phosphovanadates, in order to evaluate the effect of different VO_4^{3-} concentrations in the YPO_4 host on the spectroscopic properties of the obtained powders. To this end, a previously presented organic–inorganic polymeric precursors methodology[17] has been modified and applied to the synthesis of the crystalline solids, because this technique produces finely divided powders with high stoichiometric control of the solids. The powders were characterized with regard to their structural, morphological, and spectroscopic features, and control of their luminescent properties was achieved through variation of the vanadate concentration.

Experimental

The solids were prepared by using a variation of a previously described method starting from polymeric precursors.[17] Briefly, 1.0 mol L^{-1} rare earth nitrate solutions ($Y_{0.99}Eu_{0.01}(NO_3)_3$) were prepared by dissolving the previously calcinated oxides (Y_2O_3 99.99% Alfa-Aesar and Eu_2O_3 99.99% Rhône-Poulenc/Rhodia) in concentrated nitric acid. The pH of these solutions was regulated to ~4. The precursor of orthophosphate ions was tripolyphosphoric acid ($H_5P_3O_{10}$), which was produced from an aqueous sodium tripolyphosphate solution ($Na_5P_3O_{10}\cdot 6H_2O$ Synth 99%, previously recrystallized five times with methanol) by using a cation exchange resin (Dowex 50W X4 100–200 mesh, J.T. Baker). The $H_5P_3O_{10}$ solutions were standardized by means of potentiometric titrations with NaOH solutions immediately before their use. The source of orthovanadate ions was ammonium metavanadate (NH_4VO_3 99.9%, Aldrich). The procedures were conducted by employing different molar P/V ratios, namely 100/0, 99/1, 95/5, 90/10, 80/20, 50/50, and 0/100. For this purpose, the desired amount of the $RE(NO_3)_3$ solution was mixed with citric acid (CA) and ethylene glycol (EG) at a RE^{3+}/CA/EG molar ratio of 1/20/80, and with the appropriate volumes of the $H_5P_3O_{10}$ and/or NH_4VO_3 solutions, so that the RE^{3+}/(P + V) = 1.00 molar ratio would be attained. The final RE^{3+} concentration was adjusted to 0.02 mol L^{-1} by addition of deionized water. The clear and yellowish solution achieved at the end of this procedure was then heated at ~100 °C under stirring for 1 h, which furnished a polymeric resin. The decomposition of the resin was started in a hot plate at 400 °C and finished with calcination at 900 °C in air for 4 h, thus yielding the nanosized powders ($Y_{0.99}Eu_{0.01}(P_{1-x}V_x)O_4$, x = 0.01, 0.05, 0.10, 0.20, 0.50, and 1.00).

The morphology of the solids was evaluated by scanning electron microscopy (SEM) on Zeiss EVO 50 equipment. The structural analysis was performed by powder X-ray diffractometry (XRD) on a Siemens D5005 diffractometer. The Fourier transform infrared (FT-IR) and Raman spectra were respectively acquired on a Shimadzu IRPrestige-21 spectrophotometer (using KBr pellets, with a 2 cm^{-1} resolution) and on a Horiba LabRAM HR Raman spectrometer (using a He–Ne laser at 632.8 nm as excitation). The luminescence spectra and lifetimes were recorded on a Horiba Jobin Yvon SPEX Triax 550 Fluorolog 3 spectrofluorometer, as previously described.[23] Interference and long-pass filters were positioned in the excitation and/or emission beams, in order to improve the quality of the acquired spectra. The low-temperature luminescence spectra (77 K) were acquired by placing the samples into quartz tubes in a quartz Dewar flask filled with liquid N_2.

Results and discussion

Fig. 1 displays the SEM micrographs of some of the obtained powders; the remaining micrographs are presented in the ESI.† The images show that all solids have very similar morphology, as a result of similar conditions employed in the synthesis. Despite the high annealing temperature, which culminated in a partial coalescence process, the obtained phosphovanadates occurred as micrometric aggregates of well-defined spherical nanoparticles (~50 nm). Besides, the procedures led to a relatively narrow particle size distribution in all cases, allowing for further comparisons between structural and spectroscopic properties of the attained powders.

Fig. 2 depicts the X-ray diffractograms of the solids obtained with different vanadium(v) concentrations. Because both pure and anhydrous YPO_4 and YVO_4 have the same body-centered zircon/xenotime-type tetragonal structure, with the $I4_1/amd$

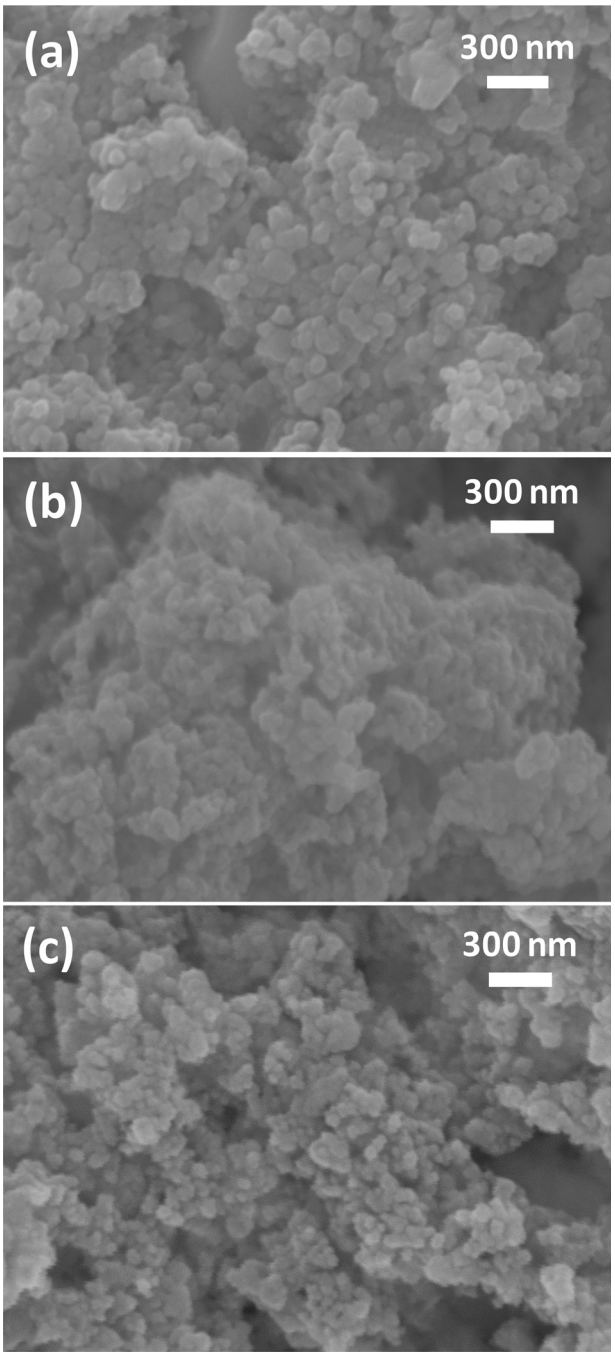

Fig. 1 SEM micrographs of some of the synthesized powders: (a) $YPO_4:Eu^{3+}$, (b) $Y(P_{0.80}V_{0.20})O_4:Eu^{3+}$, and (c) $YVO_4:Eu^{3+}$.

(D_{4h}^{19}, n° 141) space group, complete incorporation of vanadium(v) into the YPO_4 host lattice should be expected. Indeed, the diffractograms are in agreement with their standards (YPO_4 JCPDS 01-074-2429 and YVO_4 JCPDS 00-017-0341), which demonstrates that all solids exhibit the same tetragonal structure. They also evidence the absence of crystal phases related to contaminants, as well as good incorporation of the activator ions into the hosts. The relative intensity of the diffraction peaks points to the occurrence of preferential growth in the (2 0 0) plane of the tetragonal structure for the samples containing intermediate vanadium concentrations. The effect of the

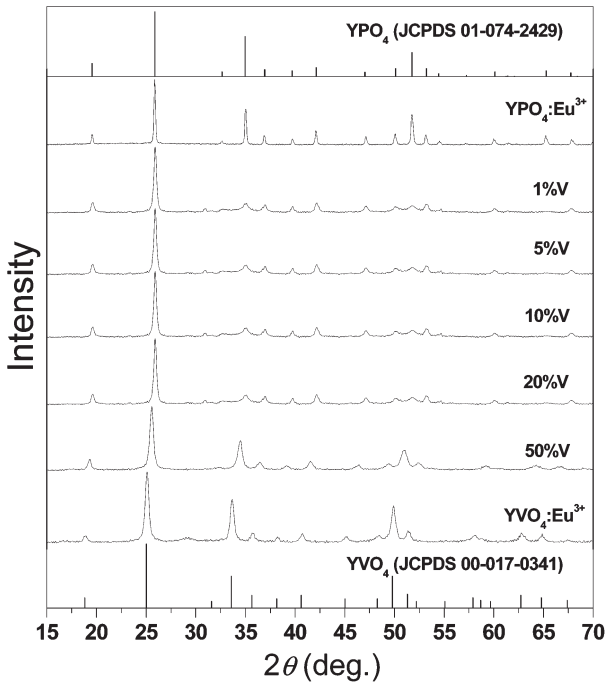

Fig. 2 X-ray diffractograms of the synthesized phosphovanadates with different vandium(v) concentrations.

Table 1 Cell parameters and crystallite sizes calculated for the synthesized tetragonal phosphovanadates

	a (Å)	c (Å)	V (Å^3)	T (nm)
$Y(P_{1-x}V_x)O_4:Eu^{3+}$, x =				
0	6.879 ± 0.005	6.016 ± 0.001	285	14
0.01	6.878 ± 0.005	6.027 ± 0.003	285	24
0.05	6.883 ± 0.005	6.030 ± 0.001	286	28
0.10	6.901 ± 0.004	6.037 ± 0.002	287	20
0.20	6.930 ± 0.015	6.046 ± 0.003	290	14
0.50	7.032 ± 0.223	6.156 ± 0.089	304	20
1.00	7.104 ± 0.006	6.274 ± 0.004	317	21

vanadium(v) ions on the structure is clearly seen by the shift of the diffraction peaks to lower 2θ values, a result of larger ionic volume of the VO_4^{3-} groups as compared to that of PO_4^{3-}. For better evaluation of this effect, the lattice parameters were calculated for the synthesized tetragonal solids (Table 1). As predicted, the introduction of the vanadate groups into the phosphate lattice results in the progressive increase of these parameters and the cell volumes. Moreover, the cell parameters of the pure phosphate (a = 6.879, b = 6.016) and vanadate (a = 7.104, b = 6.274) samples are slightly smaller than those of the YPO_4 and YVO_4 JCPDS standards (a = 6.881, b = 6.017, and a = 7.1192, b = 6.2898, respectively). The mean crystallite sizes of the prepared powders were also estimated (Table 1) from the X-ray diffractograms by applying the Debye–Scherrer relation (eqn (1)):

$$T = \frac{K\lambda}{\beta_{1/2}\cos\theta} \quad (1)$$

in which λ is the X-ray wavelength, θ is the considered Bragg diffraction peak, $\beta_{1/2}$ is the half-height peak width, and K is the shape parameter (considered to be equal to 0.9, since the particles are spherical). Within the limitations of the employed methodology, the values were close to a mean value of ~20 nm, attesting to the nanostructural character of the synthesized powders. It is also important to mention that the crystallite sizes are not necessarily equal to the observed particle sizes, since they correspond to the size of the ordered (crystalline) domains in the solid structures; thus, they assume values that are less than or equal to the grain sizes observed by microscopy techniques.[24]

The IR and Raman spectra (Fig. 3 and 4) also show the achievement of tetragonal solids and display the sets of bands typical of tetrahedral groups (orthophosphate and orthovanadate) distorted to a D_{2d} symmetry, in accordance with the $I4_1/amd$ structure.[25,26] In the pure phosphate IR spectrum (Fig. 3), the broad band with two components centred at ~1050 cm^{-1} is ascribed to the P–O anti-symmetric stretching (ν_3, B_2 + E), whereas the doublet with bands at 648 and 524 cm^{-1} is related to the anti-symmetric deformation (ν_4, B_2 + E) in PO_4^{3-} groups.[25,26] With the addition of increasing amounts of vanadate groups, a band at ~860 cm^{-1} (ν_3 stretching of VO_4^{3-}) appears and becomes more intense. In the Raman spectra (Fig. 4), besides the ν_3 and ν_4 IR-active vibrations, the symmetric stretching (ν_1, A_1) and symmetric deformation (ν_2, A_1 + B_1) of the tetrahedral groups under D_{2d} symmetry can also be observed.[26,27] The ν_1 signal occurs as a single peak at 1001 cm^{-1} in the pure phosphate and at ~891 cm^{-1} in the pure vanadate; the doublet corresponding to the ν_2 signal appears as superposed bands at ~484 cm^{-1} in the pure phosphate, and at 377 cm^{-1} in the vanadate. However, at low vanadium(V) concentrations, a broad background band is detected in the Raman spectra, which is probably a result of the VO_4^{3-} luminescence. As further discussed, the vanadate groups present more efficient luminescence when they are diluted into the YPO_4 lattice. As the vanadate emissions are quenched at higher concentrations, the luminescence becomes less intense in such cases and does not cause interference in the Raman spectra.

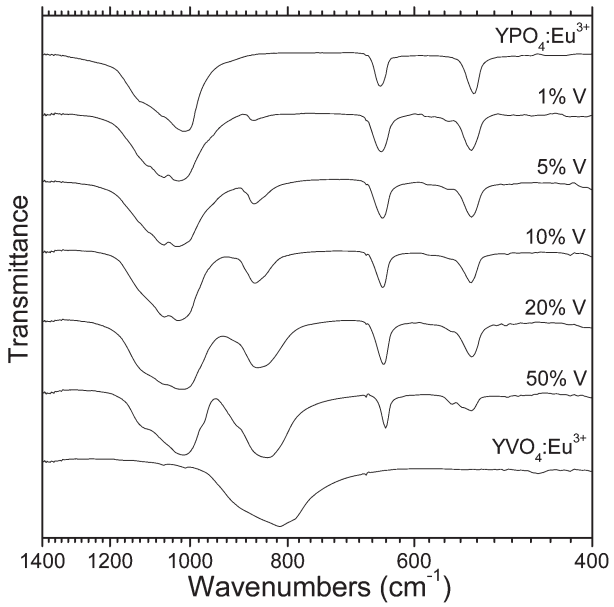

Fig. 3 FT-IR spectra (in KBr pellets) of the obtained phosphate–vanadate powders with different compositions.

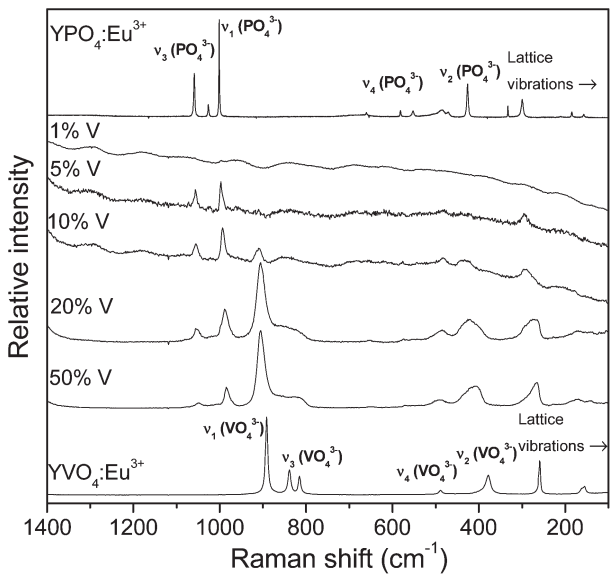

Fig. 4 Raman spectra of the obtained powders for the different vanadate concentrations.

The luminescence spectra of the synthesized solids were acquired at 300 and 77 K (liquid N_2) and are presented in Fig. 5–7 and in the ESI.† In the excitation spectra of the YPO_4:Eu^{3+} sample, the most prominent signals are attributed to the Eu^{3+} f–f absorptions, although a broad charge transfer band (CTB) can be observed at 231 nm. The addition of small vanadium(V) amounts into the YPO_4 host leads to a red-shift of the excitation band, which becomes more intense with regard to the intraconfigurational Eu^{3+} absorptions. The increase in the vanadium(V) concentration results in a progressive bathochromic shift of the excitation band, as seen in Fig. 5. The position of the ligand–metal CTB in crystalline host lattices is affected by the covalence, coordination number, bond polarizability, and anion charge. The effect of the combination of these factors can be numerically accounted for in the spectroscopic behaviour through the so-called environmental factor (h_e), which is characteristic for each host lattice. The energy relative to the maximum of the CTB is exponentially related to the environmental factor, as pointed out in eqn (2):[28]

$$E_{CTB} = A + Be^{-kh_e} \quad (2)$$

where A, B and k are experimental parameters that depend only on the nature of the lanthanoid cation. For trivalent europium, A = 2.804, B = 6.924, and k = 1.256.[28] Because the CTB energies for the obtained phosphates/vanadates range from 231 nm (5.37 eV) for YPO_4:Eu^{3+} to 311 nm (3.99 eV) for YVO_4:Eu^{3+}, the calculated environmental factors range from 0.790 to 1.405, respectively (Table 2). These values are as high as those found for Eu^{3+} ions in RE oxychlorides or oxybromides.[28] Because higher h_e values correspond to more covalent and polarizable environments, it can be concluded that the addition of increasing amounts of vanadium(V) culminates in a lower ionic character in the solids. Therefore, the difference in the CTB energies can be

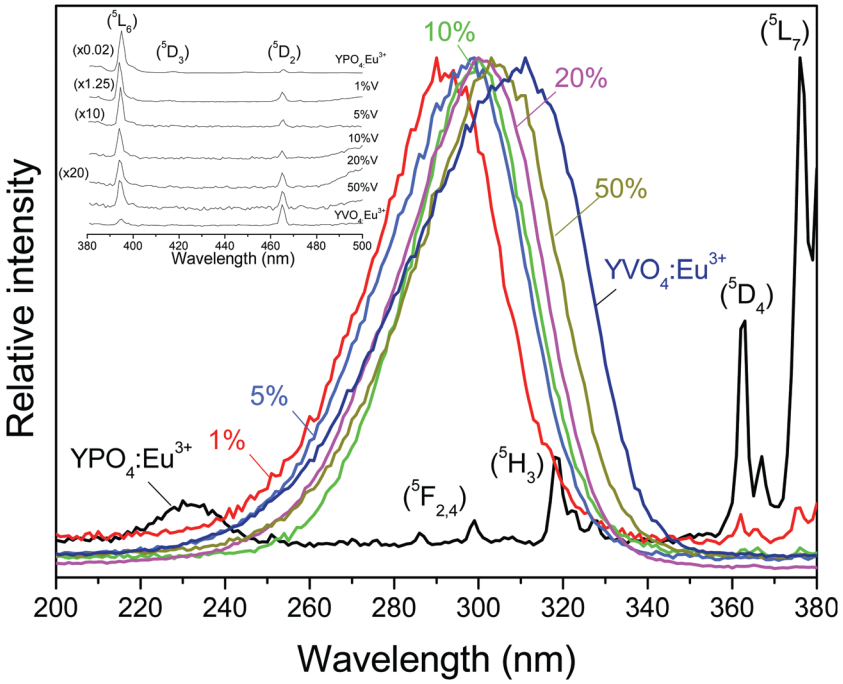

Fig. 5 Normalized excitation spectra (λ_{em} = 616 nm) of the prepared $Y(P_{1-x},V_x)O_4:Eu^{3+}$ phosphors (inset: excitation spectra in the 380–500 nm range showing the main Eu^{3+} f–f absorptions and their relative intensity with regard to the main spectra).

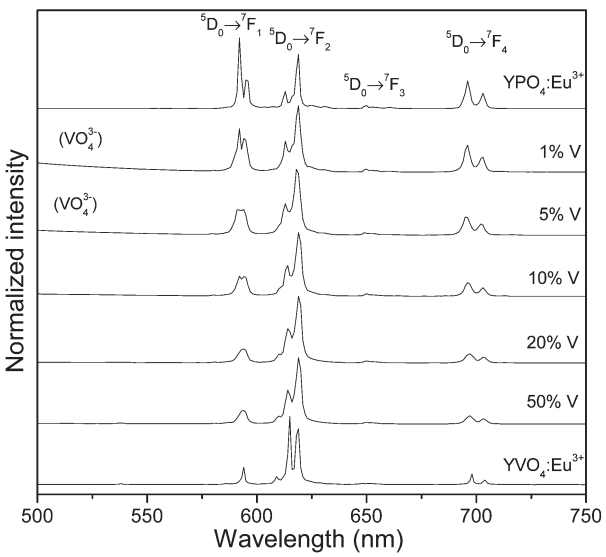

Fig. 6 Emission spectra of the obtained phosphovanadate powders for the different vanadium(v) concentrations (λ_{exc} = 394 nm for the YPO_4:Eu^{3+} sample; the remaining were excited under their CTB maxima).

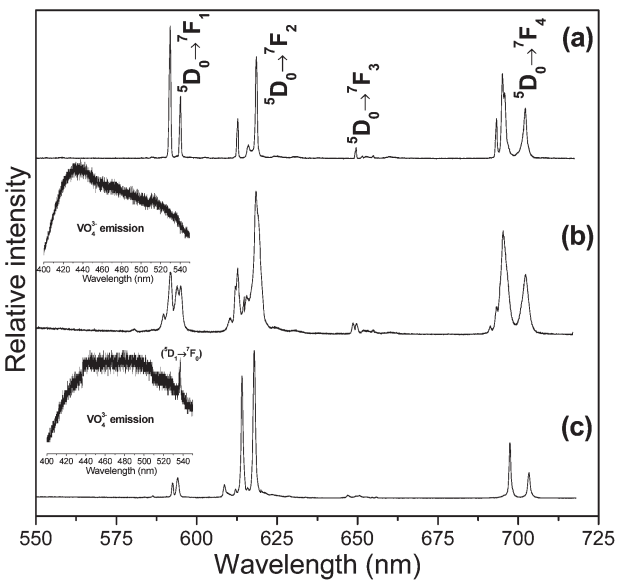

Fig. 7 Emission spectra at 77 K (liquid N_2) of (a) $YPO_4:Eu^{3+}$ (λ_{exc} = 394 nm), (b) $Y(P_{0.95}V_{0.05})O_4:Eu^{3+}$ (λ_{exc} = 300 nm), and (c) $YVO_4:Eu^{3+}$ (λ_{exc} = 310 nm) (insets: amplification of the 400–550 nm range showing the blue vanadate emissions in the two cases).

explained by taking the energy of the first 5d state of Eu^{3+} and of the O^{2-} ligands in the different cases into account, as illustrated in Fig. 8. In the pure phosphate, the energy of the CTB can be considered as the energy difference between the valence band of the host lattice and the $4f^7$ state of the europium ion; *i.e.*, the energy necessary for the formation of the bivalent state of the lanthanoid, since an electron is donated from the host to the activator ($O^{2-} \rightarrow Eu^{3+}$). On the other hand, in the presence of vanadate ions, the excitation process is a result of the allowed $O^{2-} \rightarrow V^{5+}$ CT absorption, which has a higher molar absorptivity than the $O^{2-} \rightarrow Eu^{3+}$ CT process. Consequently, excited intermediate vanadium(IV) species ($3d^1$ state) are formed, leading to the population of the Eu^{3+} emitting states, and giving rise to very efficient sensitization of the Eu^{3+} luminescence. For the orbitals comprising the electronic structure of the solids, because they are shielded by the outer electrons, the Eu^{3+} 4f electrons

Table 2 Charge transfer band (CTB) energies and environmental factors (h_e) calculated from the excitation spectra of the Eu^{3+} doped phosphovanadates

	E_{CTB} (eV)	h_e
$Y(P_{1-x}V_x)O_4:Eu^{3+}$, x =		
0	5.37	0.790
0.01	4.28	1.231
0.05	4.15	1.304
0.10	4.14	1.310
0.20	4.10	1.334
0.50	4.07	1.353
1.00	3.99	1.405

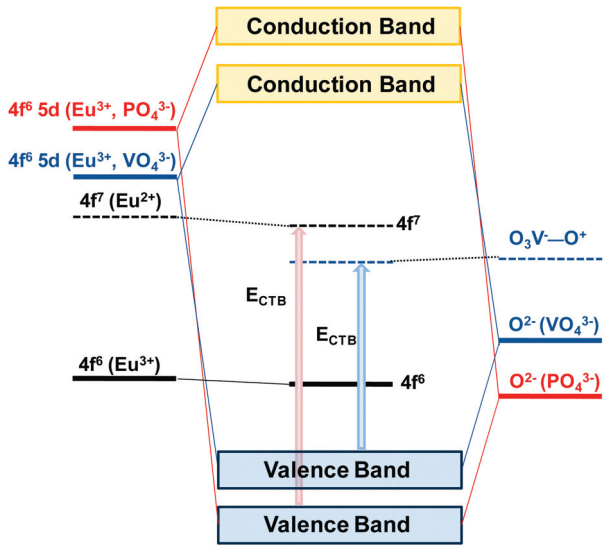

Fig. 8 Simplified energy level diagram illustrating the energy difference which gives rise to the charge transfer absorptions in the phosphate and vanadate phosphors.

poorly contribute to the formation of the valence and conduction bands, and a higher contribution is found for the Eu^{3+} 5d states. Thus, if the 5d states lie at higher energies, the generated valence band will lie at lower energies, and the energy of the CTB will increase. The introduction of the vanadate groups into the phosphate lattice results in a higher covalence, thereby culminating in a larger ligand field splitting of the 5d levels. As a consequence, the first 5d states will be at lower energies at higher vanadium(v) concentrations. Moreover, the energy of the ligands (formally O^{2-} ions) will also be affected by the differences between the PO_4^{3-} and VO_4^{3-} groups. Because they have higher bond energy, lower bond length, and higher force constant, P–O bonds are much more stable than the V–O bonds. Hence, the orbitals in the O^{2-} ions that participate in the formation of the valence and conduction bands will lie at higher energies in the presence of larger vanadium(v) concentrations. The differences between the CTB energy in the prepared phosphovanadates result from the different position of the valence bands with regard to the first charge transfer state, which is predominantly $4f^7$ ($O^{2-} \rightarrow Eu^{3+}$) in the pure phosphate, whereas it is $3d^1$ ($O^{2-} \rightarrow V^{5+}$) in the phosphovanadates. The rise in the vanadium(v) concentration leads to higher covalence in the solids, which reflects in a high lying valence band and reduces the energy difference for a charge transfer process.

Another aspect of the excitation spectra that agrees with the former conclusions is the relative intensity of the $^5D_2 \leftarrow {}^7F_0$ absorption at 464 nm in the different solids, as depicted in Fig. 5. When compared to the $^5L_6 \leftarrow {}^7F_0$ line, which is the most prominent 4f–4f excitation in the $YPO_4:Eu^{3+}$ sample, the $^5D_2 \leftarrow {}^7F_0$ transition is progressively intensified with the addition of vanadate groups. In the pure vanadate, it becomes the most intense Eu^{3+} intraconfigurational absorption. The $^5D_2 \leftarrow {}^7F_0$ transition is, as well as the $^5D_0 \rightarrow {}^7F_2$ transition, hypersensitive to the site symmetry and to the characteristics of the occupied chemical environment.[3] As pointed out in the discussion of the calculated spectroscopic parameters, the intensification of these hypersensitive transitions is associated with the occurrence of transition mechanisms other than the typical forced electric dipole in the presence of VO_4^{3-} groups, as a result of the higher polarizability of the environment around the Eu^{3+} ions in the phosphovanadates. Thus, the behaviour of the $^5D_2 \leftarrow {}^7F_0$ excitation line corroborates the observation of more covalent and polarizable sites at higher vanadate concentrations, as highlighted in the discussion of the CTB energies.

The emission spectra (Fig. 6) of the obtained solids under UV excitation exhibit the characteristic $^5D_0 \rightarrow {}^7F_J$ Eu^{3+} transitions, which occur as a set of sharp lines. Although all solids possess the same crystal structure, as demonstrated by the XRD analysis, the elevation in the vanadium(v) concentration changes the Eu^{3+} emission profile drastically. Because the synthesized solids have the xenotime-type $I4_1/amd$ structure regardless of the presence of vanadium(v), it is expected that the Eu^{3+} ions occupy D_{2d} sites in all cases. In such situations, as well as in the case of higher site symmetries, the $^5D_0 \rightarrow {}^7F_0$ transition tends to be non-observable due to the lower degree of relaxation of the spin, parity and $\Delta J \neq 0 \leftrightarrow 0$ selection rules.[3,4] This is in agreement with the observations from the emission spectra, since in all the cases the $^5D_0 \rightarrow {}^7F_0$ transition has very low intensity. Nevertheless, as seen in the low-temperature emission spectra (Fig. 7 and ESI†), intermediate vanadium(v) concentrations give rise to more than one chemical environment for the Eu^{3+} ions in the synthesized solids. Whereas for $YPO_4:Eu^{3+}$ and $YVO_4:Eu^{3+}$ only two components in the $^5D_0 \rightarrow {}^7F_1$ transition are observed, in agreement with the occupation of a single D_{2d} site by the Eu^{3+} ions, the intermediate samples clearly display four signals for such transition when higher spectral resolutions are utilized. The same occurs for the $^5D_0 \rightarrow {}^7F_2$ transition. Thus, although YVO_4 and YPO_4 can form solid solutions with a unique crystal structure in all studied proportions, the microenvironments around Eu^{3+} are slightly inhomogeneous for the intermediate cases, thereby providing two distinct D_{2d} sites for the cations in the $Y(P_{1-x}V_x)O_4:Eu^{3+}$ solids.

Another important observation is that, even under CTB excitation, involving the $O^{2-} \rightarrow V^{5+}$ electron transfer absorption, there is no significant blue luminescence of the VO_4^{3-} anions at room temperature when the vanadium(v) concentration is higher than 10%. This attests to an efficient energy transfer process between these groups and the Eu^{3+} ions. At 300 K, only in the less concentrated samples (1% and 5% V) a vanadate blue emission is observed. In these cases, a low degree of concentration quenching occurs since the absorbed energy cannot migrate

Table 3 Luminescence lifetimes, radiative and non-radiative decay rates, quantum efficiencies ($^5D_0$ level), intensity ratio between the $^5D_0 \rightarrow {}^7F_2$ and $^5D_0 \rightarrow {}^7F_1$ transitions, Judd–Ofelt intensity parameters, and chromaticity coordinates of the Eu^{3+} doped phosphovanadates[a]

	τ (ms)	A_{RAD} (s^{-1})	A_{NRAD} (s^{-1})	η (%)	I_{02}/I_{01}	Ω_2 ($\times 10^{-20}$ cm^2)	Ω_4 ($\times 10^{-20}$ cm^2)	Chromaticity	
								x	y
$Y(P_{1-x}V_x)O_4:Eu^{3+}$, x =									
0	2.8	259	99	72	0.9	1.6	2.2	0.662	0.336
0.01	2.7	334	36	90	1.8	3.0	1.9	0.428	0.272
0.05	2.2	384	70	85	2.4	4.0	1.7	0.486	0.281
0.10	1.9	440	87	84	3.0	5.1	1.9	0.553	0.302
0.20	1.4	662	62	91	5.1	8.5	2.4	0.629	0.313
0.50	1.2	669	165	80	5.3	9.0	2.2	0.645	0.316
1.00	1.0	943	98	91	8.4	13.7	2.4	0.667	0.317

[a] Luminescence lifetimes are accurate within 5%; the calculated parameters are accurate within 10%.

between the VO_4^{3-} groups. Due to elimination of the vibrational effects, at 77 K the vanadate emission becomes prominent in all cases (ESI†). The occurrence or not of the vanadate luminescence in the room temperature emission spectra is quite relevant with respect to the purity of the red emission colour of the solids, which would be lower with the broad blue vanadate emission. The chromaticity coordinates (CIE 1931) have been calculated[29] from the room temperature emission spectra, and are presented in Table 3 and Fig. 9. In the case of $YPO_4:Eu^{3+}$, a very pure red colour is achieved (x = 0.662, y = 0.336), despite the high relative intensity of the orange $^5D_0 \rightarrow {}^7F_1$ emissions. In this case, the absence of broad band emissions below 570 nm and the high relative intensity of the $^5D_0 \rightarrow {}^7F_4$ transitions in the deep red region result in a good overall chromaticity for this phosphate. In the phosphovanadate powders, the increase of the vanadium(v) concentration leads to a reduction of the blue emissions and to a progressive rise in the red $^5D_0 \rightarrow {}^7F_2$ emissions in relation to the orange $^5D_0 \rightarrow {}^7F_1$ ones, as also depicted in Table 3 (I_{02}/I_{01} ratio). As a result, the purity of the red emissions of the obtained powders can be continuously augmented from a "magenta-type" colour in $Y(P_{0.99}V_{0.01})O_4:Eu^{3+}$ (x = 0.428, y = 0.272) to very pure red in $YVO_4:Eu^{3+}$ (x = 0.667, y = 0.317) by the addition of different vanadium(v) concentrations.

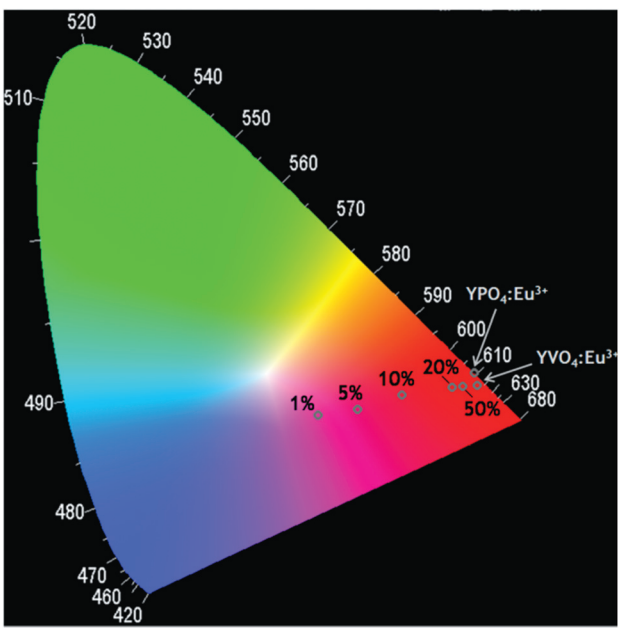

Fig. 9 CIE 1931 chromaticity diagram showing the dependence of the emission colour with regard to the vanadium(v) concentration in the synthesized powders.

Table 3 also lists the other spectroscopic parameters obtained for the Eu^{3+}-doped samples. The luminescence lifetimes ($^5D_0$ level, monitored at the $^5D_0 \rightarrow {}^7F_2$ transition) were attained by fitting the experimental decays with monoexponential decay curves. The radiative and non-radiative decay rates (A_{RAD} and A_{NRAD}, respectively) as well as the $^5D_0$ quantum efficiencies were computed from the emission spectra and luminescence lifetimes by taking the magnetic dipole allowed $^5D_0 \rightarrow {}^7F_1$ transition as a reference, as described in previous works and in eqn (3)–(8).[23,30] In summary, the emission quantum efficiency (η) of a particular excited state is defined as the ratio between the rate of radiative deactivation and the total rate of deactivation:

$$\eta = \frac{A_{RAD}}{A_{RAD} + A_{NRAD}} \quad (3)$$

The total rate of excited state deactivation ($A_{RAD} + A_{NRAD}$) is equal to the reciprocal of the experimental excited state lifetime (τ):

$$A_{RAD} + A_{NRAD} = \tau^{-1} \quad (4)$$

So, the quantum efficiency can be written as

$$\eta = A_{RAD}\tau \quad (5)$$

When the $^5D_0$ level of Eu^{3+} is considered as the emitting state, the radiative rate of excited state deactivation is equal to the sum of the particular rates for each of the $^5D_0 \rightarrow {}^7F_J$ (J = 0–6) transitions:

$$A_{RAD} = \sum_J A_{0-J} \quad (6)$$

Because of its magnetic dipole character, the $^5D_0 \rightarrow {}^7F_1$ transition has a calculable rate of radiative deactivation and can be used as a reference for the determination of the other A_{0-J} rates, and its value is given by

$$A_{0-1} = 0.31 \times 10^{-11} n^3 \sigma_{0-1}^3 \quad (7)$$

where n is the refractive index of the material and σ_{0-1} is the energy baricentre of the $^7F_1$ level (calculated from the emission spectra). The refractive index considered for our calculations was $n = 1.8$, the value usually found for xenotime. The other A_{0-J} radiative rates are calculated from

$$A_{0-J} = A_{0-1}\frac{S_{0-J}\sigma_{0-1}}{S_{0-1}\sigma_{0-J}} \quad (8)$$

where σ_{0-J} is the energy baricentre of the ^7F_J level and S_{0-J} is the area corresponding to the $^5D_0 \rightarrow {}^7F_J$ transition in the emission spectra.

Finally, the Judd–Ofelt intensity parameters (Ω_λ) are calculated by applying eqn (9):[30–33]

$$A_{0-J} = \frac{4e^2\omega^3}{3\hbar c^3}\frac{n(n^2+2)^2}{9}\sum_{\lambda=2,4}\Omega_\lambda\langle {}^5D_0\|U^{(\lambda)}\|{}^7F_J\rangle^2 \quad (9)$$

where e is the elementary charge, c is the speed of light, and $\hbar$ is the Planck constant over 2π (the three in cgs units). ω is the angular frequency of the considered transition (in cm^{-1}) and n is the refractive index. The square reduced matrix elements $<{}^5D_0\|U^{(2)}\|{}^7F_2>^2$ and $<{}^5D_0\|U^{(4)}\|{}^7F_4>^2$ have tabulated values which are, respectively, 0.0032 for the $^5D_0 \rightarrow {}^7F_2$ transition and 0.0023 for the $^5D_0 \rightarrow {}^7F_4$ transition.[30–33]

The first consideration with regard to the results summarized in Table 3 is the large increase in the I_{02}/I_{01} ratio with the addition of higher vanadium(v) amounts. Many authors try to interpret this ratio as an indication of the centrosymmetric character of the occupied site, since the intensity of the $^5D_0 \rightarrow {}^7F_1$ transition is virtually constant (magnetic dipole allowed), and the $^5D_0 \rightarrow {}^7F_2$ transition is hypersensitive to the presence of an inversion centre, which results in low intensities in such cases.[3,4] This is in fact correct, but it must be borne in mind that not only the symmetry affects this ratio. The present results are a clear example that the symmetry alone does not govern the I_{02}/I_{01} ratio, because all the solids display the same tetragonal structure, and thus D_{2d} sites are occupied in all cases. If the I_{02}/I_{01} ratio depended only on the centrosymmetric character, it would be high when the P/V ratios were close to unity, since these conditions correspond to the most inhomogeneous environments, and it would be low at both pure compositions. However, this is not observed. The results clearly demonstrate that the I_{02}/I_{01} intensity ratio is also intrinsically related to the chemical nature of the occupied sites, thus being affected by the polarizability and covalence of the ligand–metal bonds. In this sense, the comparison of I_{02}/I_{01} ratios in terms of the symmetry is only valid when ligands with very similar properties are around the Eu^{3+} ions, which seems to be not the case here.

The behaviour of the luminescence lifetimes and of the radiative and non-radiative decay rates in relation to the composition of the solids also points to more polarizable chemical environments around Eu^{3+} at higher vanadium(v) concentrations. As depicted in Fig. 10, the $^5D_0$ luminescence lifetimes are reduced from 2.8 ms in the YPO_4:Eu^{3+} sample to 1.0 ms in the YVO_4:Eu^{3+} sample, thus revealing an increase in the overall decay rate of this excited state. On the other hand, the $^5D_0$ quantum efficiencies are practically independent of the vanadium(v) concentration, within the experimental error, and present values

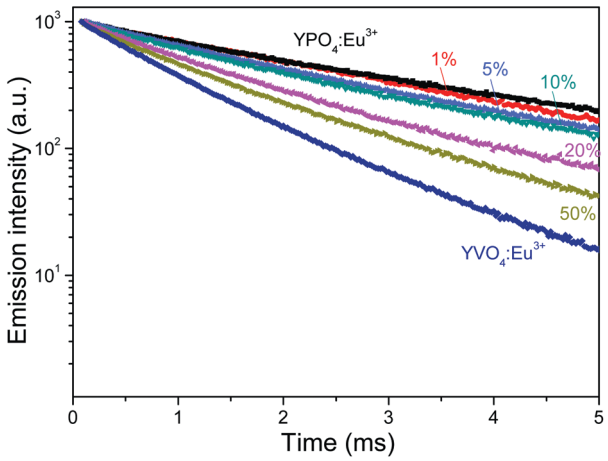

Fig. 10 Luminescence decay curves ($^5D_0$ level, monitored at the $^5D_0 \rightarrow {}^7F_2$ transition) of the $Y(P_{1-x}V_x)O_4$:Eu^{3+} powder phosphors with different vanadium(v) concentrations.

around 87 ± 7%. So it can be inferred that the shorter excited state lifetimes are not a consequence of the relative increase of non-radiative decay mechanisms, such as multi-phonon deactivation or interactions with structural defects. Therefore, the enhancement in the total decay rate without reduction in the quantum efficiency can be interpreted as the result of a higher relaxation of the selection rules in the presence of higher vanadium(v) contents. This can be explained by considering the dynamic coupling mechanism for 4f–4f transitions.[34] This mechanism is related to the occurrence of local transient electric dipoles, which are induced by the incident radiation on the electrons of the ligands, and these induced fields around the lanthanoid ions can explain the intensification of some hypersensitive 4f–4f transitions. The interaction between these induced dipoles and the metal transition quadrupole moment results in non-zero transition moments in such cases. Although this effect is obviously dependent on the site symmetry, even being forbidden in the presence of inversion symmetry, the higher is the induced electric dipole, the higher is the contribution of the dynamic coupling for the overall intensity of the spectra. Because the intensity of the local induced fields is proportional to the polarizability of the occupied chemical environment, more polarizable sites result in higher contributions of the dynamic coupling mechanism. In the present case, the introduction of larger amounts of vanadate groups into the phosphate host culminates in an increased polarizability of the Eu^{3+} sites, which reflects in a larger dynamic coupling contribution, thereby relaxing the selection rules for the involved transitions and increasing the total decay rates.

The proposed conclusions are in agreement with the calculated Judd–Ofelt intensity parameters (Ω_λ). The Ω_2 parameter is related to the degree of covalence and polarizability of the chemical environment experienced by the Eu^{3+} ion; higher Ω_2 values point to more covalent and polarizable environments.[31–35] In the prepared solids, there is a progressive increase in the Ω_2 values with the increase in the vanadium(v) concentrations, thus confirming a higher covalence and polarizability for larger vanadate contents. For the highest vanadium(v) concentrations, for example, the Ω_2 values are as high as those found for some Eu^{3+}

β-diketonates.[32,33] This is because the PO_4^{3-} groups are harder than the VO_4^{3-} ones, due to the higher stability of the P–O bonds. So, higher vanadium(v) concentrations result in more polarizable chemical environments and in more covalent RE–O bonds. On the other hand, the Ω_4 parameters are smaller than the Ω_2 ones and have close values in all cases. Some authors have attempted to relate the value of the Ω_4 parameter with the rigidity of the occupied chemical environment, which seems to be correct for many Eu^{3+} coordination compounds.[32,33,35] In the present case, the occurrence of crystalline solids and the structural similarity between all the obtained powders attest to very close site rigidities in all cases. This reflects on close Ω_4 values, which are practically the same within the experimental error.

Conclusions

In summary, the polymeric precursors method has been successfully applied for the obtainment of nanosized phosphovanadate red phosphors with different VO_4^{3-} concentrations. Despite the expected alterations introduced by the vanadate groups to the structural parameters, such as the increase in the unitary cell dimensions, all solids have the same tetragonal structure, and YPO_4 and YVO_4 could form solid solutions in all cases. Moreover, the luminescence characteristics of the obtained solids, such as emission colour, red-to-orange ratio, luminescence lifetime, and excitation maxima, can be controlled by the vanadium(v) concentration in the yttrium phosphate host. This is quite important with regard to the possible applications of these phosphors in visualization or illumination devices, so that the luminescent properties can be adapted to the required features in each case. Furthermore, these spectroscopic observations could be intrinsically correlated to the chemical characteristics in each case, and it can be concluded that the introduction of higher vanadate amounts into YPO_4 leads to a more polarizable chemical environment around Eu^{3+} and to more covalent RE–O bonds.

Acknowledgements

The authors thank the Brazilian agencies CAPES, CNPq (Proc. 480003/2009-2, O.A.S.; 146809/2011-4, J.C.B.), inct-INAMI, and FAPESP (Proc. 2008/09266-5, P.C.d.S.F.) for financial support and scholarships. The authors are also grateful to professors J.M.A. Caiut and S.J.L. Ribeiro for the Raman spectra, and Drs R.F. Silva and C.M.C.P. Manso for helpful discussions.

Notes and references

1 (*a*) C. Feldmann, T. Jüstel, C. Ronda and P. Schmidt, *Adv. Funct. Mater.*, 2003, **35**, 511; (*b*) T. Jüstel, *Nanoscale*, 2011, **3**, 1947.
2 H. A. Höppe, *Angew. Chem., Int. Ed.*, 2009, **48**, 3572.
3 (*a*) G. Blasse and B. C. Grabmaier, *Luminescent Materials*, Springer, Berlin, 1994; (*b*) J.-C. G. Bünzli, in *Lanthanide Probes in Life, Chemical and Earth Sciences*, ed. J.-C. G. Bünzli and G. R. Choppin, Elsevier, Amsterdam, 1989, ch. 7.
4 *Phosphor Handbook*, ed. W. M. Yen, S. Shinoya and H. Yamamoto, CRC Press, Boca Raton, 2nd edn, 2007.
5 (*a*) B. Moine and G. Bizarri, *Mater. Sci. Eng., B*, 2003, **105**, 2; (*b*) K. Toda, *J. Alloys Compd.*, 2006, **408–412**, 665; (*c*) T. Jüstel and H. Nikol, *Adv. Mater.*, 2000, **12**(7), 527.
6 C. Ronda, *Luminescence: From Theory to Applications*, Wiley, Weinheim, 2008.
7 C. H. Huang, G. Zhang, M. Wei, L. X. Huang, X. J. Huang and H. Y. Shen, *Opt. Commun.*, 2003, **224**, 1.
8 X. Meng, L. Zhu, H. Zhang, C. Wang, Y. Chow and M. Lu, *J. Cryst. Growth*, 1999, **200**, 199.
9 G. Panayiotakis, D. Cavouras, I. Kandarakis and C. Nomicos, *Appl. Phys. A*, 1996, **62**, 483.
10 L. Niinistö and M. Leskelä, in *Handbook on the Physics and Chemistry of Rare Earths*, ed. K. A. Gschneidner, Jr and L. Eyring, Elsevier, Amsterdam, 1987, ch. 59.
11 H. D. Nguyen, S. Mho and I. H. Yeo, *J. Lumin.*, 2009, **129**, 1754.
12 (*a*) J.-F. Dechézelles, G. Mialon, T. Gacoin, C. Barthou, C. Schwob, A. Maître, R. A. L. Vallée, H. Cramail and S. Ravaine, *Colloids Surf., A: Physicochem. Eng. Asp.*, 2011, **373**, 1; (*b*) M. Yu, J. Lin and J. Fang, *Chem. Mater.*, 2005, **17**(7), 1783.
13 D. C. Yu, M. Y. Peng, Q. Y. Zhang, J. R. Qiu, J. Wang and L. Wondraczek, *Sol. Energ. Mater. Sol. Cells*, 2011, **95**, 1950.
14 (*a*) X. Li, M. Yu, Z. Hou, G. Li, P. Ma, W. Wang, Z. Cheng and J. Lin, *J. Solid State Chem.*, 2011, **184**, 141; (*b*) Z. Hou, P. Yang, C. Li, L. Wang, H. Lian, Z. Quan and J. Lin, *Chem. Mater.*, 2008, **20**(21), 6686.
15 M. Yu, J. Lin, Y. H. Zhou, M. L. Pang, X. M. Han and S. B. Wang, *Thin Solid Films*, 2003, **444**, 245.
16 Y.-S. Chang, F.-M. Huang, Y.-Y. Tsai and L.-G. Teoh, *J. Lumin.*, 2009, **129**, 1181.
17 P. C. de Sousa Filho and O. A. Serra, *J. Fluoresc.*, 2008, **18**, 329.
18 M. Yu, J. Lin and S. B. Wang, *Appl. Phys. A*, 2005, **80**(2), 353.
19 (*a*) W. Wang, Z. Cheng, P. Yang, Z. Hou, C. Li, G. Li, Y. Dai and J. Lin, *Adv. Funct. Mater.*, 2011, **21**(3), 456; (*b*) M. Yu, J. Lin, Z. Wang, J. Fu, S. Wang, H. J. Zhang and Y. C. Han, *Chem. Mater.*, 2002, **14**(5), 2224.
20 C. Li, Z. Hou, C. Zhang, P. Yang, G. Li, Z. Xu, Y. Fan and J. Lin, *Chem. Mater.*, 2009, **21**(19), 4598.
21 V. Buissette, M. Moreau, T. Gacoin, J.-P. Boilot, J.-Y. Chane-Ching and T. Le Mercier, *Chem. Mater.*, 2004, **16**(19), 3767.
22 J. Fang, Y. Guo, G. Lu, C. L. Raston and K. S. Iyer, *Dalton Trans.*, 2011, **40**, 3122.
23 P. C. de Sousa Filho and O. A. Serra, *J. Phys. Chem. C*, 2011, **115**(3), 636.
24 Y. Dieckmann, H. Cölfen, H. Hofmann and A. Petri-Fink, *Anal. Chem.*, 2009, **81**(10), 3889.
25 R. Kijkowska, E. Cholewka and B. Duszak, *J. Mater. Sci.*, 2003, **38**, 223.
26 K. Nakamoto, *Infrared Spectra of Inorganic and Coordination Compounds*, Wiley, New York, 4th edn, 1986.
27 G. M. Begun, G. W. Beall, L. A. Boatner and W. J. Gregor, *J. Raman Spectrosc.*, 1981, **11**(4), 273.
28 L. Li and S. Zhang, *J. Phys. Chem. B.*, 2006, **110**(43), 21438.
29 P. A. Santa-Cruz and F. S. Teles, *Spectra Lux Software v.2.0*, Ponto Quântico Nanodispositivos/RENAMI (Brazil), 2003.
30 I. L. V. Rosa, P. C. de Sousa Filho, C. R. Neri, O. A. Serra, A. T. Figueiredo, J. A. Varela and E. Longo, *J. Fluoresc.*, 2011, **21**, 1575.
31 C. A. Kodaira, H. F. Brito, O. L. Malta and O. A. Serra, *J. Lumin.*, 2001, **101**, 11.
32 G. F. de Sá, O. L. Malta, C. de Mello Donegá, A. M. Simas, R. L. Longo, P. A. Santa-Cruz and E. F. Silva, Jr, *Coord. Chem. Rev.*, 2000, **196**, 165.
33 H. F. Brito, O. L. Malta, M. C. F. C. Felinto and E. E. S. Teotônio, in *The Chemistry of Metal Enolates*, ed. J. Zabicky, Wiley-Blackwell, West Sussex, 2009, ch. 3.
34 O. L. Malta and L. D. Carlos, *Quim. Nova*, 2003, **26**, 889; S. F. Mason, R. D. Peacock and B. Stewart, *Chem. Phys. Lett.*, 1974, **29**, 149.
35 V. Divya, R. O. Freire and M. L. P. Reddy, *Dalton Trans.*, 2011, **40**, 3257.

